

PHOTOELECTRIC PROPERTIES OF A NANOCOMPOSITE DERIVED FROM REDUCED GRAPHENE OXIDE AND TiO₂

A. Zh. Zhumabekov, N. Kh. Ibrayev, and E. V. Seliverstova

UDC 538.958, 54.057, 541.143

The properties of a nanocomposite derived from reduced graphene oxide and TiO₂ obtained by hydrothermal synthesis were investigated. Nanocomposite formation was confirmed by SEM as well as Raman and IR spectroscopy. The introduction of 10% rGO into the nanocomposite leads to considerably lower resistance than found for TiO₂ itself. The combination of enhanced electrotransport, optical, and adsorption parameters of these nanocomposites leads to better photoelectrochemical characteristics than for pure titanium dioxide.

Key words: reduced graphene oxide, titanium dioxide, TiO₂-rGO nanocomposite, impedance spectrum, photoinduced current.

Titanium dioxide (TiO₂) occupies a special place among semiconductor materials in light of its unique combination of physicochemical properties such as a high melting point, chemical inertness, high efficiency in phototransformations, photostability, and rapid interband recombination of charge carriers (10⁻⁹ s) [1, 2]. Other processes related to the electrotransport of charge carriers have long characteristic times in milli- or microseconds [3]. TiO₂ with a band gap of 3.2 eV is sensitive only to light with wavelengths below 380 nm. Nevertheless, this oxide is presently one of the best photocatalysts due to its high oxidizing capacity and chemical stability in the environment [4].

In order to increase the spectral sensitivity of titanium dioxide, this semiconductor is alloyed with metals [5] as well as nonmetals [6] and is used to make composites. Also, noble metals are deposited onto the semiconductor surface [7, 8], heterojunctions and quantum dots are prepared, and sensitization using dyes is carried out [9]. These composite materials hold promise for creating highly efficient photocatalysts. The formation of composites using other semiconductors, metals, and carbon materials lowers the recombination rate, while enhancing the charge separation capacity and transport capacity of TiO₂.

Graphene and its modifications with *sp*² hybridization is commonly used in energetics and environmental metals [10] for storing solar energy and photovoltaics [11], the photoelectrochemical and photocatalytic [12] generation of hydrogen/carbon fuel, and the photocatalysis of organic impurities. In recent years, modifications have attracted great attention for improving charge separation and electron transport [13, 14]. Graphene is a highly promising material for the manufacture of photocatalysts due to its excellent heat conductance, charge carrier mobility, and large surface area.

In his first paper on the preparation of such nanocomposites, Williams et al. [15] described a synthesis using UV irradiation, during which reduction of graphene oxide (GO) is observed. These authors laid the basis for the study of nanocomposites derived from graphene and TiO₂. Later, Fan et al. [16] studied a nanocomposite obtained by three different methods, namely, UV irradiation, reduction using hydrazine, and hydrothermal procedures. The nanocomposite obtained by a

Institute of Molecular Nanophotonics, Buketov Karaganda State University, Universitetskaya St., 28, Karaganda 100028, Republic of Kazakhstan. E-mail: almar89-89@mail.ru. Translated from *Teoreticheskaya i Éksperimental'naya Khimiya*, Vol. 55, No. 6, pp. 365-372, November-December, 2019. Original article submitted July 28, 2019; revision submitted December 2, 2019.

hydrothermal method was found to be the most efficient catalyst for the generation of hydrogen. Furthermore, the concentration of graphene oxide in TiO_2 strongly affects the photocatalytic activity of the nanocomposite. A 5 : 95 mass ratio of GO and TiO_2 proved optimal.

Further studies were carried out on the effect of the calcination conditions on the nanocomposite material prepared by a sol-gel method in an atmosphere of air or nitrogen. Zhang et al. [17] showed that highly efficient photocatalytic activity is found for a TiO_2 -GO nanocomposite containing 5 mass % GO after its annealing in a nitrogen atmosphere.

In the present work, we present a simple, convenient, and nonpolluting method for the synthesis of nanoparticles consisting of reduced graphene oxide and titanium dioxide. Despite the large body of work in this field, there are yet hardly any data on the interrelationships of the photoelectrochemical and electrophysical parameters of such nanocomposite materials derived from rGO and TiO_2 .

A hydrothermal method was used to synthesize a nanocomposite derived from reduced graphene oxide (rGO) and TiO_2 differing in the concentration of the components. The addition of rGO to TiO_2 should presumably improve its photoelectrochemical parameters not only due to enhanced adsorption capacity but also decreased resistance to charge transfer of the nanocomposite material in comparison with the pure semiconductor.

For the preparation of the TiO_2 -rGO nanocomposite material, we used reduced graphene oxide (rGO, from Sigma Aldrich), TiO_2 ($d > 21$ nm, 99.7% anatase, from Sigma Aldrich), deionized water (purified using the AquaMax water purification system), and anhydrous ethanol. Film deposition was carried out onto the surface of glass slides with an FTO coating (fluorine-doped tin oxide, $\sim 7 \Omega/\text{sq}$ from Sigma Aldrich). The Solaronix HI-30 iodolyte electrolyte and Solaronix Meltonix film were used to assemble cells for carrying out the electrophysical measurements. All the reagents were analytically-pure and used without further purification.

The morphology of the surface of the resultant composite materials was studied on a Tescan Mira-3 scanning electron microscope (SEM). The Raman spectra were taken using a Sol Instruments Confotec MR520 confocal microscope with laser excitation at 632.8 nm. The FTIR spectra of the composite material were taken on an Infracpec FSM 1201 (Russia). The electronic absorption spectra of the nanocomposite films were taken on an Agilent Cary-300 spectrophotometer.

Films made with pure TiO_2 or the synthesized nanocomposite on plates made of solid nonluminescing quartz were prepared to measure the absorption and Raman spectra. Determination of the width of the band gap was carried out according to Pant et al. [18] by constructing a tangent to the edge of the absorption band of the semiconductor and finding the point of its intersection with the abscissa. The error in the determination of the band gap width was ± 0.01 eV.

Powders of the materials studied were pressed into pellets for the IR spectra. Prior to use, all the parts directly contacting the samples were thoroughly washed with solvent and wiped dry.

The porous structure and specific surface were studied by the Brunauer-Emmett-Teller (BET) method using the META Sorbi-MS system. Nitrogen was used as the adsorbate. The measurement was carried out at liquid nitrogen temperature (77 K). The error in the determination of the specific surface area was $\pm 0.6 \text{ m}^2/\text{g}$.

Samples were irradiated using a Photo Emission Tech Cell Tester Model #CTAAA xenon lamp with output $100 \text{ mW}/\text{cm}^2$ (manufactured in the USA) in a standard two-electrode cell employing an Elins Z-500PRO impedance meter to study the kinetics of charge carrier transport and recombination. The amplitude of the applied signal was 25 mV and the frequency range was from 1 to 100 mHz. Platinum films deposited electrochemically from an ethanol solution of H_2PtCl_6 solution onto glass plates with a conducting FTO layer were used as the pick-up electrode. The electrodes were glued to each other. The spacer between the working electrode and the pick-up electrode was a Meltonix polymer film. Iodolyte was used as the electrolyte. The irradiated area was 0.16 cm^2 . The volume of the electrolyte in the cells as well as the thickness and area of the films were identical in all the samples. The impedance spectra were analyzed using the EIS analyzer program.

A study of the junction characteristics of the photocurrent of the materials obtained was carried out by recording the photoinduced current in a standard three-electrode photoelectrochemical cell with a quartz window in an Elins P-30J potentiostat-galvanostat. Ag/AgCl was used as the reference electrode. A diode lamp with output $35 \text{ mW}/\text{cm}^2$ was employed as the irradiation source. The samples studied were deposited by centrifugation onto the surface of plates coated with FTO, which were connected to the working electrode. A platinum electrode was connected to a negative potential. The measurements were carried out in 0.1 M aqueous NaOH.

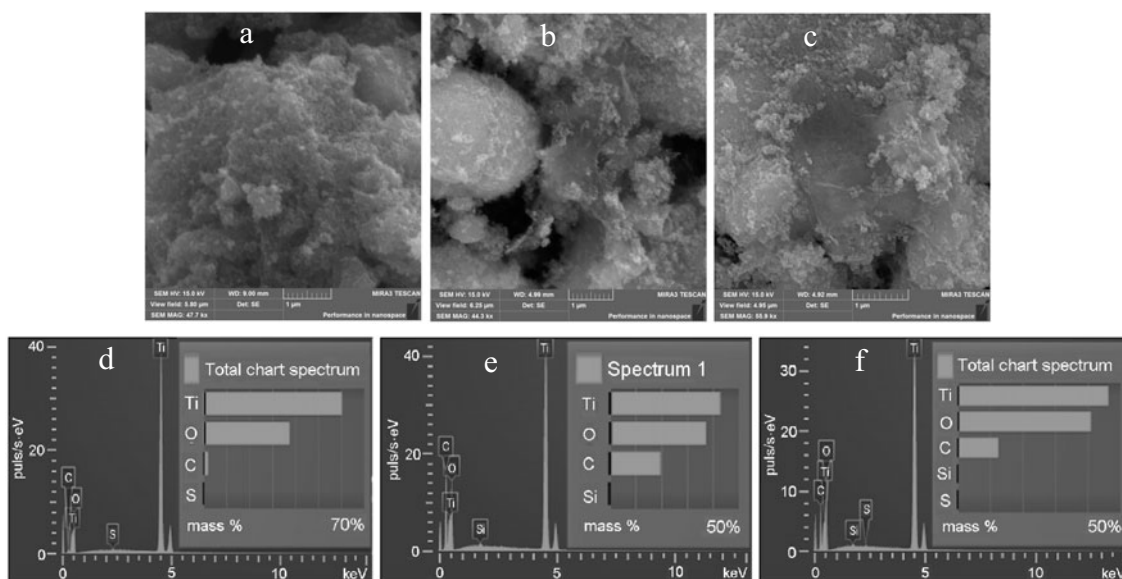


Fig. 1. SEM images (a-c) and energy-dispersive X-ray diffraction (d-f) of nanocomposite material: a, d) TiO_2 -rGO/1%, b, e) TiO_2 -rGO/5%, and c, f) TiO_2 -rGO/10%.

The TiO_2 -rGO nanocomposite was prepared as follows: 10 mg reduced graphene oxide (1 mass % relative to TiO_2) was mixed with 30 mL deionized water and 10 mL ethanol. The suspension was then subjected to ultrasonic treatment for 1 h. Subsequently, 1 g TiO_2 was added and ultrasonic treatment was alternated with shaking for 2 h (30 min for each procedure) until a homogeneous light gray suspension was obtained. The suspension was then placed into a Teflon-coated autoclave and left for 24 h at 120 °C to prepare the composite. After cooling to room temperature, the suspension was filtered several times using deionized water. The resultant product was dried at 60 °C. A similar procedure was carried out in the synthesis of materials with reduced graphene oxide concentration of 5 and 10 mass %.

Films consisting of the TiO_2 -rGO nanocomposite were prepared from a paste of the synthesized powder and ethanol by centrifugation. The films were deposited onto the surface of FTO-coated plates. After deposition and drying, the films were annealed in an argon atmosphere for 2 h at 450 °C.

SEM images of the nanocomposite material with reduced graphene oxide concentration of 1, 5, and 10 mass % are given in Fig. 1a-c, which show that the nanoparticles are aggregated in the bulk titanium dioxide sample. Pores between the particles can be discerned in these images.

Reduced graphene oxide has a layered structure formed by individual sheets. The graphene oxide sheets tend to form wrinkles and folds, which is clearly seen in Fig. 1, b and c. The TiO_2 nanoparticles concentrate precisely at these sites. Lv et al. [19] have shown that this occurs because oxygen-containing groups are retained in large amounts at these sites, through which a strong interaction takes place between reduced graphene oxide and titanium dioxide.

In addition, the presence of reduced graphene oxide in the synthesized sample was confirmed by EDXS analysis (Fig. 1d-f), which showed that the carbon content increases with increasing concentration of reduced graphene oxide.

SEM studies showed that reduced graphene oxide is spread out throughout the entire TiO_2 -rGO composite. This permits the TiO_2 particles upon the action of light to inject their photogenerated electrons into the rGO sheets for efficient transport to the FTO layer and subsequent recording.

Figure 2a gives FTIR spectra for the TiO_2 -rGO nanocomposite with different mass ratios of the starting materials. The IR spectra obtained were analyzed using the data of various authors [18, 20, 21]. In particular, the IR spectrum of reduced graphene oxide shows vibrational bands of bonds, which can be assigned to the following chemical groups: C–O (1095 cm^{-1}), C–O–C (1261 cm^{-1}), C–OH (1454 cm^{-1}), C=O (1728 cm^{-1}). The strong peak at 3441 cm^{-1} characterizes vibrations of the O–H groups in C–OH and water. The peak arising at 1628 cm^{-1} is presumably related to skeletal vibrations of reduced graphene

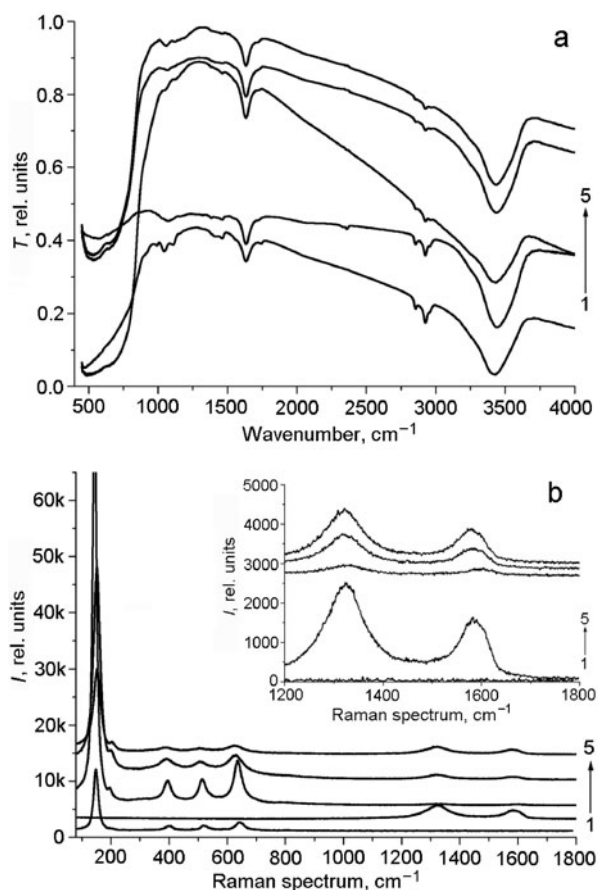


Fig. 2. IR (a) and Raman spectra (b) of samples: 1) TiO₂, 2) rGO, 3) TiO₂-rGO/1%, 4) TiO₂-rGO/5%, and 5) TiO₂-rGO/10%.

oxide according to Zhang et al. [21] and may also be assigned to deformation vibrations of adsorbed water molecules, whose presence is indicated by broad strong band with maximum at about 3400 cm⁻¹.

Pure TiO₂ shows a low-frequency mode at about 500 cm⁻¹, which corresponds to Ti–O–Ti bond vibrations. The spectrum also shows a strong band at 3440 cm⁻¹, which indicates that –OH groups are adsorbed on the surface of titanium dioxide particles.

The IR spectrum of the TiO₂-rGO nanocomposite shows absorption below 1000 cm⁻¹. Vasilaki et al. [20] have shown that this peak may be considered as a combination of Ti–O–Ti (695 cm⁻¹) and Ti–O–C bond vibrations (near 792 cm⁻¹). However, the latter band is not clearly pronounced and has low intensity. Nevertheless, Vasilaki et al. [20] have indicated that absorption in this region for this type of nanocomposites can be an indication of binding of titanium dioxide and rGO during hydrothermal synthesis, leading to the formation of the TiO₂-rGO nanocomposite material. Furthermore, functional groups for rGO (bands below 1500 cm⁻¹) are partially absent in the spectra of the nanocomposite, which is evidence for the reduction of graphene oxide after the synthesis.

Raman spectra of the synthesized samples were taken to obtain additional confirmation of the reduction of graphene oxide during the hydrothermal synthesis (Fig. 2b).

The anatase structure of titanium dioxide has six Raman-active peaks (Fig. 2b), including three *E_g* peaks centered at 149, 183, and 630 cm⁻¹ (*E_g*(1), *E_g*(2), and *E_g*(3), respectively), two *B_{1g}* peaks at 397 and 506 cm⁻¹ (designated *B_{1g}*(1) and *B_{1g}*(2)) as well as an *A_{1g}* peak at 481 cm⁻¹ [22].

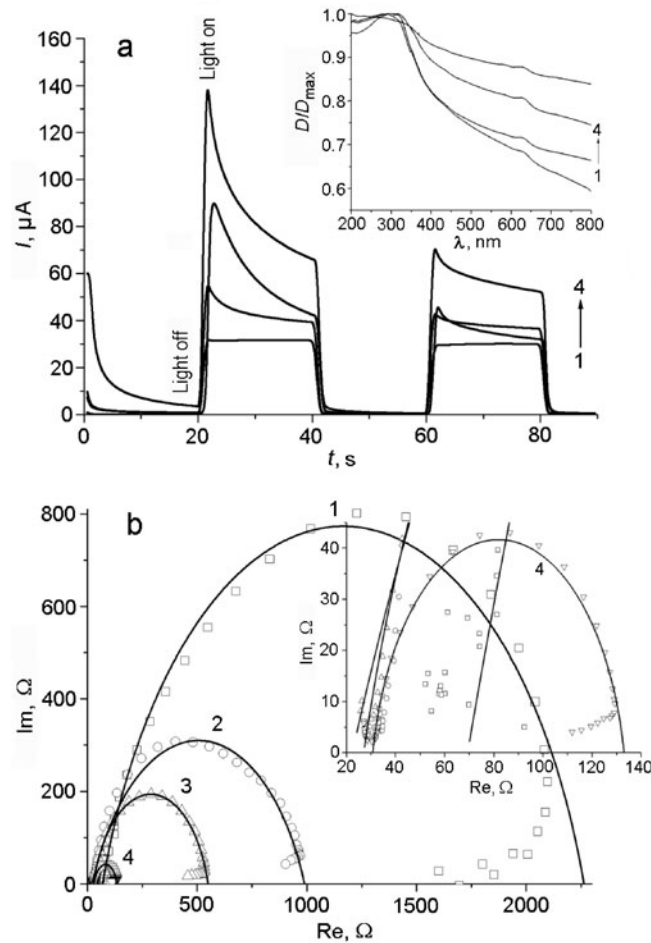


Fig. 3. Transitional characteristics of the photocurrent of samples (a) (insert gives the absorption spectra) and Nyquist plot of the impedance spectrum (b): 1) TiO₂, 2) TiO₂-rGO/1%, 3) TiO₂-rGO/5%, and 4) TiO₂-rGO/10% (insert gives Nyquist plot for the impedance spectrum for TiO₂-rGO/10% in an enlarged scale).

The spectrum of reduced graphene oxide has two characteristic bands. The D band in the vicinity of 1330 cm^{-1} characterizes the defectivity of graphene and is active only when the defects participate in double resonance scattering near the Brillouin zone. The G band is centered at about 1590 cm^{-1} . The I_D/I_G intensity ratio is equal to 1.56 ± 0.05 .

The Raman spectra of the nanocomposite are a combination of the spectra of the individual components. The ratio of the intensities of the D and G bands (I_D/I_G) with increased rGO concentration in the nanocomposite is 1.54 ± 0.05 , 1.46 ± 0.05 , and 1.45 ± 0.05 for 1, 5, and 10 mass %, respectively. The decrease in this parameter (from $I_D/I_G = 1.56$) at high reduced graphene oxide concentrations indicates the reduction of graphene oxide during the synthesis [23], which is supported by the IR spectral data.

The photocatalytic activity of the TiO₂-rGO and TiO₂ nanocomposite materials was examined. The photocurrent intensity was measured over 20 s with cyclical switching on and off of the light. We should note that Fig. 3a shows the dependence of the generation and recombination of the photocurrent of TiO₂-rGO and TiO₂ films upon elapsed time. The shape of the photogenerated current curve may be explained as follows [24]: switching on the light leads to very rapid photoinduced separation of the electron-hole pairs, which is seen as a peak on the photocurrent curve. Then, this flash fades out since the charge carriers migrate to the film surface (electrons to FTO and holes to the electrolyte). The subsequent decrease in the

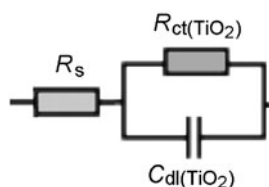


Fig. 4. Equivalent electrical scheme of the electrochemical cell.

photocurrent indicates that recombination occurs within the film. A longer time period is required by the charge carriers generated deep within the film to reach the surface than for the carriers generated near the surface. The extent of predominance of recombination in the generation of charge carriers determines the rate of photocurrent attenuation. A constant photocurrent is achieved when rates of charge carrier generation and recombination become equal. In the case of TiO_2 , in which all the charge carriers have the same lifetime, the rates of these processes are apparently similar and, thus, the photocurrent curves have an almost rectangular shape.

Figure 3 shows that the increase in the photocurrent of the TiO_2 film is $\sim 30 \mu\text{A}$ and this value is repeated at each onset of irradiation by the light source. This is the lowest value of the photocurrent relative to the other samples. The photocurrent is enhanced by a factor of 1.5 upon irradiation of the TiO_2 -rGO/1% sample. Similar results were obtained for nanocomposites TiO_2 -rGO/5% ($62 \mu\text{A}$) and TiO_2 -rGO/10% ($87 \mu\text{A}$). These values are 2.0 and 2.9 times greater than for pure TiO_2 . Since the efficiency of the photocatalytic dissociation of water into molecular oxygen and hydrogen depends on the amount of photoinduced electrons, hydrogen generation when using TiO_2 -rGO/10% will be greater than for the other similar nanocomposites.

The improvement of the photoelectrochemical activity may be related both to better charge transport properties of the semiconductor in the presence of graphene and a consequence of the large specific surface of the nanocomposite. Furthermore, we should bear in mind that the visible spectral sensitivity of the nanocomposites is somewhat higher than for a film of pure titanium dioxide.

The insert in Fig. 3a shows absorption spectra of the nanocomposites and pure TiO_2 . The edge of the absorption band of TiO_2 in the UV spectrum appears at about 400 nm. Reduced graphene oxide also absorbs in the UV range and the maximum of its absorption spectrum is at 230 nm. In addition, broadening of the absorption band in the visible spectrum is seen. Zhang et al. [25] have shown that this effect is related to change in the band gap width of the semiconductor in these nanocomposite materials. The band gap width of the hybrid TiO_2 -rGO composite decreases from $3.26 \pm 0.01 \text{ eV}$ (TiO_2) to $2.52 \pm 0.01 \text{ eV}$ (TiO_2 -rGO/10%). The smaller band gap width and enhanced absorption in the visible region due to modification of rGO should lead to greater photocatalytic activity of the TiO_2 -rGO hybrid nanocomposite.

Studies have also been carried out on the electrophysical characteristics of these nanocomposite materials using various procedures [26-28]. Nyquist plots of the impedance spectra for films of these nanocomposites with different rGO concentration in the nanocomposite and of TiO_2 itself are shown in Fig. 3b. In order to analyze the experimental curves and evaluate the electrotransport properties of the films, a simplified equivalent electrical scheme for an electrochemical cell was used (Fig. 4); this is a special case of a scheme taken from the work of Zhang et al. [29].

Zhang et al. [29] have presented an equivalent electrical scheme consisting of three consecutively-connected Randles contours, which is seen in the Nyquist plot as three ideal semicircles. According to these authors, the first contour corresponds to the FTO/ TiO_2 and FTO/Pt separation boundary, while the second corresponds to the TiO_2 /electrolyte separation boundary and the third corresponds to the Pt/electrolyte separation boundary. Figure 3b shows in our case that the impedance spectra of the samples are mostly represented by a single semicircle. Hence, we used the scheme shown above. The simplified electrical scheme was used to model the spectra of TiO_2 and TiO_2 -rGO.

The resultant impedance spectra were used to calculate the major electrotransport properties of the films. Parameters such as R_k , R_w , k_{eff} , and τ_{eff} were also determined, where R_k is the resistance to charge transfer related to electron-hole

TABLE 1. Electrotransport Properties of Films of TiO₂ and TiO₂-rGO with Different rGO Concentrations

Sample	R_k, Ω	R_w, Ω	k_{eff}, S	$\tau_{\text{eff}}, \text{ms}$
TiO ₂	2194.0 ± 1.42%	69.3 ± 15.82%	13.895 ± 15%	72 ± 15%
TiO ₂ -rGO/1%	967.3 ± 1.27%	22.4 ± 26.38%	99.957 ± 15%	10 ± 15%
TiO ₂ -rGO/5%	522.9 ± 0.5%	27.1 ± 4.68%	51.767 ± 15%	19 ± 15%
TiO ₂ -rGO/10%	102.2 ± 1.14%	30.7 ± 2.09%	26.822 ± 15%	37 ± 15%

recombination, R_w is the resistance to electron transport in the TiO₂-rGO film, k_{eff} is the effective rate of charge carrier recombination, and τ_{eff} is the effective electron lifetime.

The data obtained from the impedance spectra permit evaluation of the charge carrier recombination passing through traps found on levels close to the conduction band.

When the impedance arc is part of a proper circle, the values of R_k considerably exceed the values of R_w [30], which is confirmed by the data in Table 1. The addition of reduced graphene oxide reduces the resistances R_k and R_w of the semiconductor samples. The value of R_k is reduced by a factor of 20 with increasing concentration of reduced graphene oxide to 10 mass %. The insert in Fig. 3b shows that TiO₂-rGO with 10 mass % rGO has a value of R_k equal to 102.2 Ω . The value of R_w subsequently increases with increasing mass of graphene oxide to 10 mass % relative to TiO₂.

The data in Table 1 show that an increase in the mass fraction of rGO in the nanocomposite leads to increased conductance of the material. A further increase in the mass fraction of rGO decreases the amount of TiO₂. This, in turn, decreases the amount of photoelectrons generated in TiO₂. In particular, this would be seen in rather high rates of charge carrier recombination in the nanocomposite bulk comparable to the values obtained by Adachi et al. [30]. Thus, there is an optimal concentration of the added reduced graphene oxide in the semiconductor.

We assume that the addition of 1 mass % reduced graphene oxide leads to an increase in the photocurrent as well as improved transport properties of TiO₂ due to electron displacement through the rGO sheets. The amount of reduced graphene oxide in the TiO₂-rGO nanocomposite with 1 and 5 mass % rGO is insignificant. Thus, excited electrons cannot move fully along the rGO sheets. Movement of charge carriers is possible over much longer distances in rGO with 10 mass % rGO in comparison with other samples. Thus, lower resistance was found for the nanocomposite with 10 mass % rGO. Similar results were obtained by Bell et al. [24], who showed that the conductance of films is higher in the presence of rGO at the optimal concentration. This behavior is related not only to decreased resistance of these samples but also increased effective electron lifetime.

The absorption properties of the nanocomposite material were also studied by the BET method. Table 2 gives the results of measurement of the specific surface area calculated by this method. The specific surface area of powdered reduced graphene oxide is nine times greater than for the other samples. The specific surface areas of pure TiO₂ and the nanocomposite material with 1 mass % rGO are almost identical.

Increasing the concentration of reduced graphene oxide in the powder leads to enhanced adsorption capacity up by a factor of 1.67 to $89.6 \pm 0.6 \text{ m}^2/\text{g}$. After preparation of the paste and annealing in an argon atmosphere, the specific surface of the TiO₂-rGO nanocomposite is enhanced by factors of 1.37, 1.53, and 1.67 for 1, 5, and 10 mass % rGO, respectively, in comparison with the values for films of pure TiO₂. Table 2 shows that the greatest specific surface is found for the TiO₂-rGO/10% nanocomposite.

Thus, these studies have shown that hydrothermal synthesis can lead to formation of a bond between the TiO₂ particles and sheets of reduced graphene oxide and TiO₂-rGO nanocomposites. The IR spectra show that the functional groups characteristic for reduced graphene oxide have partially disappeared in the TiO₂-rGO nanocomposites, which indicates further reduction of this oxide during the synthesis.

The Raman spectra of the nanocomposite are a combination of the spectra of the individual components. The ratio of the intensities of the *D* and *G* bands of graphene oxide decreases with increasing rGO concentration in the nanocomposite

TABLE 2. Specific Surface Area of Pure Reduced Graphene Oxide, TiO₂, and TiO₂-rGO Nanocomposites with Different rGO Concentrations

Samples	$S_{\text{BET}}, \pm 0.06 \text{ m}^2/\text{g}$	
	Powder	Film
rGO	425.3	–
TiO ₂	53.5	67.3
TiO ₂ -rGO/1%	73.1	80.3
TiO ₂ -rGO/5%	81.7	85.8
TiO ₂ -rGO/10%	89.6	92.6

material. This hypothesis is further supported by the IR spectral data. EDXS analysis also showed the presence of titanium, oxygen, and carbon in the powdered nanocomposite material.

Measurements of the optical characteristics of the synthesized material showed that the absorption spectrum of the TiO₂-rGO nanocomposite is shifted toward longer wavelengths relative to the absorption spectrum of the starting components. This shift might be the result of a change in the band gap width of the semiconductor.

Studies of the electrophysical parameters have shown that the addition of rGO to TiO₂ leads to a 20-fold decrease in the resistance R_k and R_w of the semiconductor material. Increasing the mass fraction of rGO in the nanocomposite leads to an increase in conductance. A further increase in the mass fraction of rGO enhances the amount of photoelectrons generated in TiO₂. Furthermore, the addition of reduced graphene oxide to the semiconductor leads to a 60% increase in the specific surface area of the resultant samples.

The combined increase in both the electrotransport as well as the optical and adsorption parameters of the nanocomposites leads to improvement of their photoelectrochemical characteristics in comparison with titanium dioxide without added rGO. The greatest increase in the photocurrent by a factor of 2.9 is observed when the rGO concentration in the film is 10 mass %.

These results may be used for creating a highly-efficient catalyst sensitive to visible light for the photocatalytic degradation of organic compounds.

This work was carried out in the framework of Grants AP05132443 and BR05236691 financed by the Ministry of Education and Science of the Republic of Kazakhstan.

REFERENCES

1. A. B. Murphy, *Sol. Energy Mater. Sol. Cells*, **91**, No. 14, 1326-1337 (2007), doi: 10.1016/j.solmat.2007.05.005.
2. K. Woan, G. Pyrgiotakis, and W. Sigmund, *Adv. Mater.*, **21**, No. 21, 2233-2239, doi: 10.1002/adma.200802738.
3. I. P. Stepanenko, *Fundamentals of the Theory of Transistors and Transistor Systems* [in Russian], Énergiya, Moscow (1977).
4. Sh.-D. Mo and W. Y. Ching, *Phys. Rev. B*, **51**, No. 19, 13023-13032 (1995), doi: 10.1103/PhysRevB.51.13023.
5. S. Angkaewa and P. Limsuwana, *Procedia Eng.*, **32**, No. 1, 649-655 (2012), doi: 10.1016/j.proeng.2012.01.1322.
6. P. Calandra, A. Riggirello, A. Pistone, and V. T. Liveri, *J. Clust. Sci.*, **4**, No. 3, 767-778 (2010), doi: 10.1007/s10876-010-0330-x.

7. V. N. Kuznetsov and N. Serpone, *J. Phys. Chem. C*, **111**, No. 42, 15277-15288 (2007), doi: 10.1021/jp073511h.
8. H. Zhang, G. Wang, D. Chen, et al., *Chem. Mater.*, **20**, No. 20, 6543-6549 (2008), doi: 10.1021/cm801796q.
9. S. M. Gupta and M. Tripathi, *J. Phys. Chem.*, **56**, No. 16, 1639-1657 (2011), doi: 10.1007/s11434-011-4476-1.
10. P. V. Kamat, *J. Phys. Chem. Lett.*, **2**, No. 3, 242-251 (2011), doi: 10/1021/jz101639v.
11. X. Wang, L. Zhi, and K. Muellen, *Nano Lett.*, **8**, No. 1, 323-327 (2008), doi: 10.1021/nl072838r.
12. L. Y. Ozer, C. Garlisi, H. Oladipo, et al., *J. Photochem. Photobiol. C*, **33**, No. 12, 132-164 (2017), doi: 10.1016/j.photochemrev.2017.06.003.
13. C. Chen, W. Cai, M. Long, et al., *ACS Nano*, **4**, No. 11, 6425-6432 (2010), doi:10.1021/nn102130m.
14. Y. H. Ng, I. V. Lightcap, K. Goodwin, et al., *J. Phys. Chem. Lett.*, **15**, No. 1, 2222-2227 (2010), doi: 10.1021/jz100828z.
15. G. Williams, B. Seger, and P. V. Kamat, *ACS Nano*, **2**, No. 7, 1487-1491 (2008), doi: 10.1021/nn800251f.
16. W. Fan, Q. Lai, Q. Zhang, and Ye. Wang, *J. Phys. Chem. C*, **115**, No. 21, 10694-10701 (2011), doi: 10.1021/jp2008804.
17. Z.-Y. Zhang, H.-P. Li, X.-L. Cui, and Y. Lin, *J. Mater. Chem.*, **20**, No. 14, 2801-2806 (2010), doi: 10.1039/b917240h.
18. B. Pant, P. S. Saud, M. Mark, et al., *J. Alloys Compd.*, **671**, No. 25, 51-59 (2016), doi: 10.1016/j.jallcom.2016.02.067.
19. K. Lv, Sh. Fang, L. Si, et al., *Appl. Surf. Sci.*, **391**, No. 1, 218-227 (2017), doi: 10.1016/j.apsusc.2016.03.195.
20. E. Vasilaki, I. Georgaki, D. Vernardou, et al., *J. Appl. Surf. Sci.*, **353**, No. 30, 865-872 (2015), doi: 10.1016/j.apsusc.2015.07.056.
21. H. Zhang, X. Lv, Y. Li, et al., *ACS Nano*, **4**, No. 1, 380-386 (2010), doi: 10.1021/nn901221k.
22. Y. Swamy, A. Kuznetsov, L. S. Dubrovinsky, et al., *Phys. Rev. B*, **71**, No. 18, 184302 (2005), doi: 10.1103/PhysRevB.71.184302.
23. A. Jario, M. Dresselhaus, R. Saito, and G. F. Dresselhaus, *Raman Spectroscopy in Graphene Related Systems*, Wiley-VCH Verlag, Weinheim (2011).
24. N. J. Bell, Y. H. Ng, A. Du, et al., *J. Phys. Chem. C*, **115**, No. 13, 6004-6009 (2011), doi: 10.1021/jp1113575.
25. L. Zhang, J. Zhang, H. Jiu, et al., *J. Phys. Chem. Solids*, **86**, No. 6, 82-89 (2015), doi: 10.1016/j.jpcs.2015.06.018.
26. J. Bisquert, G. Garcia-Belmonte, F. Fabregat-Santiago, and P. R. Bueno, *J. Electroanal. Chem.*, **475**, No. 2, 152-163 (1999), doi: 10.1016/S0022-0728(99)00346-0.
27. R. Kern, R. Sastrawan, J. Ferber, et al., *J. Electrochim. Acta*, **47**, No. 26, 4213-4225 (2002), doi: 10.1016/S0013-4686(02)00444-9.
28. J. Bisquert, *J. Phys. Chem. B*, **106**, No. 2, 325-333 (2002).
29. B. Zhang, D. Wang, Y. Hou, et al., *Sci. Rep.*, **3**, No. 1, 1836-1843 (2013), doi: 10.1038/srep01836.
30. M. Adachi, M. Sakamoto, J. Jinting, et al., *J. Phys. Chem. B*, **110**, No. 28, 13872-13880 (2006), doi: 10.1021/jp061693u.